Fast three-dimensional super-resolution imaging of live cells

Sara A. Jones[1,5], **Sang-Hee Shim**[1,5], **Jiang He**[2], and **Xiaowei Zhuang**[1,3,4]

[1] Department of Chemistry and Chemical Biology, Harvard University, Cambridge, MA 02138

[2] Department of Molecular and Cellular Biology, Harvard University, Cambridge, MA 02138

[3] Department of Physics, Harvard University, Cambridge, MA 02138

[4] Howard Hughes Medical Institute, Harvard University, Cambridge, MA 02138

Abstract

We report super-resolution fluorescence imaging of live cells with high spatiotemporal resolutions using stochastic optical reconstruction microscopy (STORM). By labeling proteins either directly or via SNAP tags with photoswitchable dyes, we obtained two-dimensional (2D) and three-dimensional (3D) super-resolution images of living cells, using clathrin-coated pits and the transferrin cargo as model systems. Bright, fast switching probes enabled us to achieve 2D imaging at spatial resolutions of ~25 nm and temporal resolutions as fast as 0.5 sec. We also demonstrated live-cell 3D volumetric super-resolution imaging. A 3D spatial resolution of ~30 nm in the lateral directions and ~50 nm in the axial direction was obtained at time resolutions down to 1 – 2 sec with several independent snapshots. Using photoswitchable dyes with distinct emission wavelengths, we further demonstrated two-color 3D super-resolution imaging in live cells. These imaging capabilities open a new window for characterizing cellular structures in living cells at the ultrastructural level.

The development of super-resolution fluorescence microscopy has allowed the diffraction-limited resolution to be surpassed[1–2]. This advancement has been achieved either by spatially modulating the fluorescence emission with patterned illumination as in the cases of stimulated emission depletion microscopy (STED or RESOLFT)[1,3] and saturated structured illumination microscopy (SSIM)[4–5], or by stochastically switching individual molecules on at different times as in the case of stochastic optical reconstruction microscopy (STORM) or (fluorescence) photoactivation localization microscopy ((F)PALM)[6–8]. The latter approach further requires high-precision localization of single molecules[9–10] and photoswitchable probes. These techniques have allowed biological structures to be imaged with resolution as high as ~20 nm. Recent demonstrations of super-resolution imaging in living cells, as

Correspondence should be addressed to X.Z. (zhuang@chemistry.harvard.edu).
[5]These authors contributed equally to this work.

Competing interests statement.
The authors declare that they have no competing financial interests.

exemplified by the video-rate STED imaging of synaptic vesicles in live neurons[11], have further enabled the characterization of cellular dynamics with sub-diffraction-limit resolution.

However, due to the intrinsic trade-off between spatial and temporal resolutions, the image resolutions achieved in live cells are substantially lower than that for fixed samples where the imaging speed is not a concern. The spatial resolution reported for the video-rate live-cell STED is ~60 nm in the lateral dimensions, 3 fold larger than what has been achieved on fixed cells[11]. A recent live-cell STED study reports ~150 nm axial resolution when imaging samples in the *xz* plane[12]. Live-cell SIM has achieved ~10 Hz imaging speed in a wide field with a spatial resolution of ~100 nm in the lateral dimensions[13]. For the single-molecule-based imaging methods, such as (F)PALM or STORM, this trade-off arises from the requirement that a sufficiently large number of localizations need to be accumulated for each snapshot in order to define a structure with a desired spatial resolution. This requirement is best characterized by the Nyquist criterion which equates the image resolution to 2/(localization density)$^{1/D}$, where D = 1, 2, or 3 for one- (1D), two- (2D) or three-dimensional (3D) imaging, respectively[14]. Therefore, although photoactivation-facilitated high-density particle tracking has proven powerful for probing molecular motions in living cells[15–17], the Nyquist criterion has so far limited the spatial resolution of the single-molecule-based imaging methods to 40 – 70 nm in 2D with a 30 – 60 sec time resolution[14,18], when imaging photoactivatable fluorescent proteins in live cells. 2D super-resolution imaging has also been performed in living cells with photoswitchable dyes[19–22], but the localization density has not been characterized in these cases and thus the image resolution achieved is unclear. Because more localizations are inherently required to define a structure in 3D, it is expected that extending super-resolution imaging to 3D will further deteriorate the time resolution. Indeed, 3D (F)PALM or STORM has not yet been achieved for live cells. These limitations have significantly hindered the application of super-resolution fluorescence microscopy to the ultrastructural characterization of living cells.

Here, we report 2D and 3D super-resolution imaging of live cells with high spatial and temporal resolutions using photoswitchable dyes. We achieved a Nyquist resolution of ~20 nm with a time resolution as high as 0.5 sec for 2D STORM imaging. Moreover, 3D volumetric super-resolution imaging of live cells was achieved with an overall resolution of 30 nm in *xy* and 50 nm in *z* at time resolutions down to 1 – 2 sec, albeit with a relatively low number of independent snapshots. We demonstrated these imaging capabilities not only for exogenously added molecules, but also for intracellular proteins by delivering bright, fast switching cyanine dyes into living cells and by using genetic fusion strategies to specifically label proteins with these probes. In addition, we compared the 3D image resolutions achieved with six photoswitchable probes in live cells, including the photoswitchable cyanine dye, Alexa Fluor 647 (Alexa647), three cell permeable photoswitchable dyes, Atto655, TMR and Oregon Green, and two photoactivatable Eos fluorescent protein derivatives, mEos2 and tdEos.

RESULTS

Model system for live-cell STORM

We used the clathrin-mediated endocytic machinery as a model system to illustrate the above imaging capabilities. Clathrin-coated pits (CCPs) are responsible for the endocytosis of many cell-surface receptors and their cargos, among which transferrin is a classical example. To set the stage for live-cell imaging, we first imaged the nanoscale morphology of CCPs and the enclosed transferrin clusters in fixed cells. For this purpose, we labeled transferrin and clathrin with photoswitchable probes using two strategies. The first is based on the activation properties of probes containing the photoswitchable dye Alexa647. Specifically, transferrin was directly labeled with a photoswitchable dye pair, Alexa405-Alexa647, and clathrin was immunolabeled with another pair, Cy3-Alexa647. In this scheme, the photoswitchable Alexa647 was imaged and the probes were distinguished by the wavelength of light used to activate the dye pair[23–24]. In the second approach, two photoswitchable dyes with spectrally separable emission wavelengths were used: Alexa647 for clathrin labeling[25] and Alexa568 for transferrin labeling[19].

Among the various 3D STORM/(F)PALM approaches[26–30], we chose astigmatism imaging. In this approach, a cylindrical lens was inserted into the imaging path to render the image of each molecule elliptical; the centroid and ellipticity of the image were used to determine the lateral (x and y) and axial (z) coordinates of the molecule, respectively[26]. A 3D STORM image was then constructed from the x, y and z coordinates of all imaged molecules through iterative activation. We determined the localization precision of Alexa647 to be 7 nm in x and y, and 17 nm in z measured in standard deviation (SD), which corresponds to 17 nm in x and y, and 45 nm in z measured in full-width at half maximum (FWHM). The localization precision of Alexa568 was lower, 23 nm in x and y, and 61 nm in z (FWHM) due to its two-fold reduction in photons per switching cycle as compared to Alexa647. The localization precision changed only slightly over the 300 nm imaging depth used in this work (See Methods).

As expected, the STORM images show substantial resolution improvement over the conventional image. In the conventional images, the majority of transferrin and CCPs appeared as colocalized diffraction-limited puncta with no discernable morphological details (Supplementary Fig. 1a). In contrast, 3D STORM images show transferrin as clusters of 50–80 nm in size, enclosed by clathrin coats in the shape of a half-spherical shell of 100–200 nm in diameter (Supplementary Fig. 1b–d). In the following, we demonstrate live-cell imaging of both the exogenously added transferrin cargo and the intracellular protein, clathrin.

2D live-cell STORM with sub-second time resolution

First, we performed 2D imaging of transferrin clusters in live cells. Alexa405-Alexa647-labeled transferrin was added to cells that were serum-starved to increase the surface density of transferrin receptors, and thereby increase the number of receptors within each coated pit. The cyanine dyes, such as Alexa647, switch off to a dark state by forming a thiol-adduct in imaging buffer containing thiol[31]. We thus used beta-mercaptoethanol to support

photoswitching and an oxygen scavenger system (OSS) to reduce photobleaching, albeit at lower levels than typically for fixed cell imaging to maintain cell health. To achieve fast imaging speeds, which directly depends on the switching rate of the probes, a 657 nm laser of up to 15 kW/cm^2 (at the sample) was used to rapidly image and switch off individual Alexa647 molecules. A weak 405 nm laser, typically two to four orders of magnitude less intense than the 657 nm laser, was used to activate only an optically resolvable subset of molecules at any time. Both lasers were kept on continuously to optimize the imaging speed[32]. STORM movies were recorded with 500 Hz camera frame rate. Our control experiments showed that neither the thiol- and OSS-containing imaging buffer nor the strong laser illumination exerted significant effects on the cell morphology (Supplementary Fig. 2 and Movie 1) or transferrin uptake kinetics (Supplementary Fig. 3).

Under these conditions, individual Alexa647 molecules were switched off in ~2 camera frames on average, emitting an average of 3,500 photons per switching event (Supplementary Fig. 4). The fast switching kinetics of Alexa647 allowed us to record super-resolution images with high speed. Figure 1a shows the STORM image of transferrin clusters acquired at room temperature over a wide field of view. The zoomed-in comparison with the conventional image shows a substantial resolution improvement (Fig. 1b). Figure 1c shows six independent, 0.5-sec STORM snapshots of two example transferrin clusters. The cluster diameter and number of localizations within the clusters remained largely unchanged from snapshot to snapshot. Due to the short snapshot duration (0.5 sec), the observed size and shape of the cluster did not show significant motion blurring effects -- statistics over many clusters showed a similar cluster size distribution when compared to that obtained in fixed cells (Supplementary Fig. 5a, b).

To assess the spatial resolution of these STORM snapshots, we note that the image resolution is limited not only by the localization precision of each probe molecule, but also by the localization density within the structures. According to the Nyquist criterion, the average distance between neighboring localizations should be no more than half of the size of an object in order for the object to be resolvable. Therefore, a Nyquist resolution of 2/(localization density)$^{1/D}$ must also be considered when specifying the spatial resolution, in addition to the localization precision[14]. The measured cluster size and number of localizations within the cluster allowed us to determine the localization density for each cluster. Although each Alexa647 molecule could potentially give multiple localizations, we used the localization density to calculate the Nyquist resolution for the following two reasons. First, under our experimental conditions, the snapshot durations were shorter than or comparable to the average time between consecutive activation events of a single probe. Therefore, the localization density was comparable to the activated probe density within each snapshot. In all experiments throughout this work, the Nyquist resolution would change by 30% or less if the activated probe density was used for calculation. Second, transferrin receptors diffuse within coated pits. We measured a diffusion coefficient of 0.06 μm^2/s for transferrin within the clusters, consistent with previous results[33]. Therefore, multiple localizations of the same moving probe can be included to sample the underlying cluster shape. A similar strategy has been used to map the bacterial cytoskeleton structure with live-cell super-resolution imaging[18]. For the 0.5 sec STORM snapshots in the above examples, we determined the Nyquist resolution to be less than 20 nm (Fig. 1d). Statistics over many

transferrin clusters recorded at 0.5-sec time resolution give an average 2D Nyquist resolution of 19 nm (Fig. 1e). After convolution with the 17-nm localization precision (measured in FWHM), we obtained an overall resolution of 25 nm.

3D live-cell STORM

Most cellular structures have a 3D organization, and therefore 3D super-resolution imaging is required to resolve their ultrastructure. Considering that the localizations in this case are spread out not only in the lateral dimensions but also in the axial dimension, a larger number of localizations, and thus a longer imaging time, are needed to achieve a similar Nyquist resolution. Despite this requirement, the fast switching kinetics of Alexa647 allowed us to obtain 3D STORM images of a wide field of view with high speed. As an example, Fig. 1f shows 3D STORM snapshots of a transferrin cluster obtained every 2 sec, with a 3D Nyquist resolution of ~22 nm (Fig. 1g). Statistics over many transferrin clusters recorded at 2-sec time resolution yielded a Nyquist resolution distribution averaged at 30 nm (Fig. 1h), which, when convolved with the localization precision, gave an overall resolution of 34 nm in *xy* and 54 nm in *z*. Statistics over many clusters taken in live cells showed a similar cluster size distribution as that obtained in fixed cells, indicating a lack of significant motion blurring effects (Supplementary Fig. 5a, c). The overall imaging time was, however, relatively short at this high-speed imaging condition due to photobleaching of the probes and therefore insufficient to capture the internalization process of the transferrin cluster.

We thus reduced the activation laser intensity to decrease the on-switching rate of the probe and acquired 6-sec snapshots for a longer period of time at 34°C. Even at this time resolution and elevated temperature, the size distribution of the clusters showed minimal motion blur, with the average cluster size comparable to that obtained at 0.5 and 2 sec resolution (Supplementary Fig. 5d). As shown in Fig. 1i, the dynamics of a transferrin cluster were captured, starting from formation to disappearance. The cluster formed at ~6 sec, remained largely stationary in the lateral dimension while the *z* position increased significantly (Figs. 1i and j), and finally disappeared abruptly at ~50 sec in a single snapshot. This rapid disappearance is unlikely due to photobleaching, which would result in a more gradual decrease in the localization number as different molecules photobleach stochastically at different times. Instead, the sudden disappearance was likely due to internalization of the cluster because endocytic vesicles often embark on rapid cytoskeletal-dependent movement immediately after internalization and thereby leave the shallow imaging field[34]. Supporting this notion, statistics over multiple clusters showed that the mean disappearance time was 72 ± 14 sec, which is quantitatively comparable to the internalization time measured at 34°C for transferrin using conventional imaging methods under the same buffer and temperature conditions (Supplementary Fig. 3).

3D live-cell STORM of intracellular proteins

In the above examples, proteins of interest were directly labeled with photoswitchable dyes prior to addition to live cells. Applying a similar labeling approach to intracellular proteins, such as clathrin, would be more challenging. Instead, we employed the SNAP-tag technology[35] for specific clathrin labeling with Alexa647. To this end, we generated a fusion construct of SNAP and clathrin light chain (CLC) and transfected cells with this

construct. We then used electroporation to deliver the SNAP-reactive Alexa647 molecules (BG-Alexa647) into living cells. The distribution and dynamics of CCPs in cells expressing this dye-labeled fusion protein were similar to those expressing the previously validated EYFP-CLC fusion construct[34,36].

We first performed imaging experiments at room temperature with a relatively slow time resolution of 30 sec using low activation light intensity (Fig. 2). Conventional images of the Alexa647-labeled clathrin showed the expected punctate pattern of CCPs, which appeared as diffraction-limited spots with no discernable structure (Fig. 2a,c). In contrast, live-cell 3D STORM images resolved the nanoscopic structure of CCPs (Fig. 2b,c). The xy and xz cross-sections of individual CCPs revealed the cup-like morphology of the clathrin coat (Fig. 2c). The average 3D Nyquist resolution of CCPs observed in an entire field of view was determined to be 24 nm, which gave an overall resolution of 29 nm in xy and 51 nm in z after convolution with the localization precision of Alexa647 (Supplementary Table 1). The size distribution of CCPs determined from these 30-sec snapshots was similar to the distribution determined from both the 10-sec snapshots of live cells and the fixed cell images (Supplementary Fig. 6), indicating minimal motion-blurring effects as expected from the slow CCP dynamics at room temperature.

Increasing the 405 nm activation intensity allowed us to improve the time resolution to as fast as 1 sec while maintaining a similar Nyquist resolution at 32 nm (Fig. 2d). The observation of the non-trivial, cup-like shape of coated pits suggest that 3D STORM can indeed be used to resolve nanoscopic structures in live cells.

In addition to electroporation, other approaches can be used to deliver dye molecules into living cells. We also obtained STORM images of CCPS in live cells by delivering BG-Alexa647 using a bead-loading method (Supplementary Fig. 7)[37].

Two-color 3D STORM in live cells

By adding Alexa568-labeled transferrin to cells expressing Alexa647-labeled SNAP-CLC-fusion proteins, we also obtained two-color 3D STORM images of transferrin and clathrin in live cells (Fig. 3). The 30-second STORM images allowed us to clearly discriminate transferrin and clathrin, which appeared as completely overlapping puncta in the conventional images (Fig. 3a,b). The morphology of the clathrin coat enclosing the transferrin cluster was resolved in this nanoscopic cellular structure (Fig. 3b–d). A reduction in the resolution was observed in the transferrin channel as compared to the single color transferrin image taken with Alexa647 due to the lower number of photons detected from Alexa568 (~1,700 photons). The overall resolution became 40 nm in xy and 70 nm in z in the transferrin channel, instead of the 34 nm xy and 54 nm z resolutions obtained in the single-color cases. The resolution in the clathrin channel remained largely unchanged from the single-color cases described earlier.

Comparison with other photoswitchable probes

Given the requirement of live-cell delivery of the non-cell permeable Alexa647, we next tested several additional photoswitchable probes for live cell super-resolution imaging and

compared their performances with Alexa647. These probes include mEos2 and tdEos, two of the brightest photoactivatable fluorescent proteins[14,38–39], and three cell permeable photoswitchable dyes, Atto655, TMR and Oregon Green, which have been used previously for live cell super-resolution imaging[14,20–22]. For imaging with EosFP, we created a fusion protein of CLC and mEos2 or tdEos. For imaging with the organic dyes, the SNAP tag was used as described above for Alexa647. Among the SNAP-reactive substrates, BG-TMR and BG-Oregon Green were found to be cell permeable and were added to the cells expressing SNAP-CLC directly. BG-Atto655 was, however, not able to penetrate the cell membrane and was delivered into living cells by electroporation, as in the case of BG-Alexa647.

The 30-sec 3D STORM snapshots of CCPs labeled with these probes are shown in Supplementary Fig. 8. Among these probes, tdEos and mEos2 offered higher image quality than Atto655, TMR and Oregon Green. However, due to the relatively low number of photons detected from individual mEos2 and tdEos molecules (~1,200 photons), the image resolution obtained with these probes was not as good as that of Alexa647. The overall resolution, considering both localization precision and density, was ~40 nm in *xy* and ~80 nm in *z* for mEos2 and tdEos (Supplementary Table 1). As a result, the cup-like morphology of CCPs was no longer clearly resolved (Supplementary Fig. 8a, b). While an interferometry approach can be used to increase the image resolution, the requirement to sandwich the sample between two closely opposing objectives makes it more difficult to implement for live cells[29]. Moreover, it is difficult to increase the imaging speed substantially due to the photophysical properties of these fluorescent proteins. Unlike Alexa647, which emitted a constant number of photons per switching cycle independent of the excitation light intensity (Supplementary Fig. 4c), the number of photons emitted by an Eos fluorescent protein before switching off decreased with the excitation intensity (Supplementary Fig. 9a). The light used to image the activated form of Eos also appeared to cause bleaching of the unactivated form (Supplementary Fig. 9b), reducing the localization density at high excitation intensity. These properties prevented the use of higher light intensity to achieve a faster imaging speed.

Compared to the two fluorescent proteins, the three photoswitchable dyes, Atto655, TMR and Oregon Green, additionally suffered from lower localization density (Supplementary Table 1), leading to a further reduction in image resolution (Supplementary Fig. 8c–e and Supplementary Table 1). Because stronger illumination further reduced the number of attainable localizations, we were also unable to improve the time resolution to beyond 30 sec in these cases. For these probes with relatively low photon numbers, we also observed a moderately larger *z*-variation in the localization precision (See Methods).

To further facilitate quantitative comparison, we constructed a composite image of CCPs for each of the six probes from CCP structures detected in an entire field of view. The *xy* cross-sections of the composite CCP images and their density profiles along the *x* direction are shown in Fig. 4. The composite image of the Alexa647-labeled CCPs clearly shows a ring-like cross-section, as expected for the coated pits. Due to the broad size distribution of CCPs, the thickness of the composite ring appeared wider than our image resolution. In contrast, the hollow center of the ring structure was not clearly revealed in the tdEos and mEos2 images, which instead exhibited a top-hat profile. The profiles of the Atto655, TMR

and Oregon Green images, in particular the latter two, exhibited a Gaussian-like shape and completely failed to resolve the CCP morphology.

DISCUSSION

In order to obtain high spatiotemporal resolutions, several important parameters must be considered. First, since the super-resolution image is reconstructed from localizations of individual molecules, the localization precision is a key determinant of the image resolution. Among the six photoswitchable probes tested here, Alexa647 gives the highest photon output in each switching cycle, corresponding to a localization precision of 17 nm in xy and 45 nm in z (FWHM), which is significantly higher than those afforded by tdEos, mEos2, Atto655, TMR and Oregon Green (Supplementary Table 1). For live cell imaging, it is also important to consider how the movement of individual probe molecules within the structure may affect the localization precision. For example, under our experimental conditions, transferrin molecules diffuse by ~20 nm during the 2 ms camera frame, which should have only a moderate effect on our image resolution. Another important factor in spatial resolution is the localization density. Based on the Nyquist criterion, a sufficient number of localizations are needed to define the structure with a desired resolution in each snapshot. Since the total number of localizations is limited by the density of labels on the structure of interest and the photoswitching properties of the probe molecules, the total number of snapshots attainable is limited. Although Alexa647-labeled structures tend to give more localizations as compared to other probes, the overall number of snapshots attainable per structure is still rather limited, especially for CCPs at the high spatial resolution described here. A future challenge is to identify probes with more switching cycles under live cell imaging conditions for better characterization of ultrastructural dynamics.

For obtaining high temporal resolution, the critical factor is the photoswitching rate of the probes. Alexa647 maintains a constant photon output independent of the excitation intensity. This property allowed us to switch Alexa647 molecules rapidly with high illumination intensity and to achieve a time resolution that is two orders of magnitude higher than previously reported for single-molecule-based super-resolution imaging in living cells. Given the trade-off between time resolution and overall imaging time, it is sometimes beneficial to reduce the time resolution for probing longer processes. Reducing the time resolution by decreasing the imaging laser intensity is, however, not always desirable because a slower off-switching rate may cause degradation of the localization precision, if the probe molecules diffuse inside the structure. The adjustment in time resolution can be achieved alternatively without the above concern by tuning the on-switching rate with the activation light intensity as demonstrated here.

Finally, the choice of probe is a balancing act between desired spatial and temporal resolutions, attainable localization density, and ease of use. All six probes tested in this work provided sub-diffraction image resolution in 3D. The fluorescent proteins and cell permeable dyes have the advantage of allowing relatively easy labeling of live cells and, additionally, lower nonspecific labeling background in the case of fluorescent proteins. On the other hand, the superior brightness and faster switching kinetics of the cyanine dye Alexa647 make it the probe of choice for imaging at very high spatiotemporal resolutions.

Being a non-membrane-permeable dye, labeling intracellular proteins in living cells with this dye, however, requires not only specific labeling chemistry for cellular proteins but also nontrivial live-cell delivery of the dye molecules. In addition to the SNAP tag technology, a variety of other hybrid fusion systems can be used to link dye molecules to the protein of interest through a genetically fused peptide sequence or protein tag[20–21,40]. We have demonstrated two different dye delivery approaches, electroporation and bead loading, for STORM imaging. In particular, electroporation combines both high efficiency and reproducibility. Nonetheless, it is still a relatively laborious approach and can cause cell-to-cell variation in labeling efficiency. Future development of cell-permeable cyanine dyes is desirable to further enhance the versatility of these probes for live cell super-resolution imaging.

Numerous sub-cellular structures have nanometer-scale dimensions. The characterization of many of these structures in fixed cells is subject to fixation artifacts, especially at the ultrastructural level. We thus expect the high spatiotemporal-resolution imaging capabilities demonstrated here to substantially benefit ultrastructural characterizations in living cells.

METHODS

Cell Culture

BS-C-1 cells (CCL-26; American Type Culture Collection (ATCC)), an African Green monkey kidney epithelial cell line, were maintained in a 5% CO_2 atmosphere at 37°C in Eagle Modified Minimum Essential Medium (ATCC), supplemented with 10% FBS (Invitrogen). Cells were passaged every 2–3 days and maintained for up to 15 passages. For imaging, cells were plated into 8-well chambered coverglasses (LabTek-II; Nalgene Nunc) cleaned previously with 1M potassium hydroxide, at a density of ~ 16,000 – 30,000 cells per well depending on the experiment.

Plasmid Construction

To generate CLC-Eos plasmids, mEos2 (gift from Dr. Loren Looger and Dr. Michael Davidson) or tdEos (gift of Dr. Michael Davidson) were fused to the C-terminus or N-terminus of mouse CLC version A, respectively. mEos2 was digested out of the pmEos2-N vector using AgeI (5′) and NotI (3′) and ligated into a similarly digested, previously described pEYFmLCa vector[34,36]. An intermediate tdEos-C1 plasmid was generated by exchanging tdEos for EYFP in pEYFP-C1 (5′-NheI; 3′ – EcoRI, Clontech) and subsequently mLCa was inserted at KpnI (5′) and ApaI (3′). To generate the pEYFP-CLC-SNAP vector, SNAP26m was amplified from the pSNAP-tag(m) vector (New England Biolabs) with added XhoI (5′) and EcoRI (3′) sites, digested and then ligated into a similarly digested pEYFP-mLCa vector. The pSNAP-CLC-SNAP vector was generated by replacing the EYFP in the pEYFP-CLC-SNAP vector with SNAP26m, a PCR product from pSNAP-tag(m), with added AgeI (5′) and NotI (3′) restriction sites. We engineered the EYFP-CLC-SNAP construct for easier identification for the transfected cells with the EYFP fluorescence signal and the SNAP-CLC-SNAP construct with two SNAP tags for increased labeling density. The distribution and dynamics of CCPs in cells expressing the CLC-mEos2, tdEos-CLC and cells expressing the EYFP-CLC-SNAP and SNAP-CLC-SNAP fusion proteins were similar

to those observed in cells expressing EYFP-CLC, a fusion protein that has been previously validated to be functionally intact[34,36].

Transfection

Trypsinized cells were transiently transfected with a Nucleofector Device (Lonza) using Cell Line Nucleofector Kit V and program X-001. Transfected cells were then plated into 8-well chambered coverglasses and used for experiments 24–40 hours post-transfection. For labeling SNAP-tagged proteins with dyes delivered into live cells by electroporation, cells were first nucleofected with a combination of pSNAP-CLC-SNAP and pEYFP-CLC-SNAP constructs (3:1 ratio) for increasing label density and for easy identification of transfected cells. For two-color imaging with Alexa568-transferrin only pSNAP-CLC-SNAP was used to avoid spectral overlap. Transfected cells were then plated into a culture flask. Since nucleofection is a solution based technique, once tagged-protein expression was maximal (after ~ 18–24 hours) cells were trypsinized again and nucleofected a second time with program T-030 in the presence of 100 μM BG-Alexa647 (BG-Surface Alexa Fluor 647; New England Biolabs) or BG-Atto655 (Gift of New England Biolabs) for dye delivery. Cells were then re-plated onto 8-well chambered coverglasses, the media changed after ~ 4 hours and imaged ~ 10 – 20 hours after plating. For labeling with cell permeable dyes, ~24 hours after nucleofection with pSNAP-CLC-SNAP alone, cells were incubated for 30 minutes in 5μm BG-TMR-Star or BG-OregonGreen (New England Biolabs) diluted in culture medium[21–22]. Cells were rinsed 3 times and allowed to recover at 37°C in the absence of dye for 1–2 hours prior to imaging. Further increasing either the labeling concentration or incubation time did not result in a higher degree of labeling. For dye-delivery with the bead-loading method, cells were loaded with 425 – 600 μm acid-washed glass beads (Sigma Aldrich) as previously described[37] in 50 μM BG-Alexa647, and allowed to recover at 37°C for 30 – 60 minutes prior to imaging.

Immunostaining

Approximately 24 hours after plating cells were serum starved in Dulbecco's Modified Eagle Medium (DMEM) with high glucose and no phenol red (Invitrogen) for 60 minutes. Alexa568-labeled transferrin (5 μg/mL, Invitrogen) or Alexa405-Alexa647-labeled transferrin (20 μg/mL) was either cold bound for 10 minutes on ice followed by 37°C incubation for 2 minutes, or bound at room temperature for 2 minutes without temperature shift, prior to fixation with 4% paraformaldehyde (Electron Microscopy Sciences). Both transferrin incubation conditions gave similar results. Immunofluorescence was performed as previously described using antibodies against clathrin heavy chain (ab21679, Abcam or MA1-065, Thermo Scientific) and corresponding secondary antibody (Jackson Immunoresearch)[24,41]. For Alexa405-Alexa647-transferrin, a Cy3-Alexa647 secondary antibody was used, while for Alexa568-transferrin, an Alexa405-Alexa647-labeled secondary was used.

Live-Cell Imaging

For imaging Alexa647, cells were rinsed twice in serum free DMEM and transferred to the microscope stage. Imaging buffer was then prepared with DMEM (high glucose, no phenol red, Invitrogen) or DMEMgfp (Evrogen) supplemented with 2% glucose, 6.7% of 1M

HEPES pH 8.0, 0.5% beta-mercaptoethanol (Sigma), and an oxygen scavenging system (0.5 mg/mL glucose oxidase and 40 ug/mL catalase) was added immediately before image acquisition. mEos2, tdEos, TMR, Oregon Green, and Atto655 probes were imaged in DMEM as previously described[14,20–21]. Among these five probes, mEos2, tdEos, Atto655 gave higher imaging quality than TMR and Oregon Green. We tested whether adding OSS and beta-mercaptoethanol could further improve the image quality for these probes, but did not find them to be helpful in these cases. For imaging involving transferrin, cells were incubated in serum free DMEM for 30 – 60 minutes at 37°C. After cells were transferred to the microscope stage, Alexa405-Alexa647-transferrin or Alexa568-transferrin was added *in situ*, left for 1 min, and then diluted by 6 times with imaging buffer right before image acquisition.

To correct for sample drift, 100 nm polystyrene fluorescent beads (Fluospheres, red fluorescent; Invitrogen) were affixed to the chambered coverglass by heating at 100°C as fiducial markers[42]. The chambers were allowed to cool and rinsed extensively with water before cells were plated. Imaging experiments were performed at room temperature or at 34°C in the transferrin internalization experiment. The latter condition allows for more rapid internalization such that the internalization process could be recorded within our imaging window.

Optical setup and image acquisition

All STORM experiments were performed on an Olympus IX71 inverted optical microscope. Six laser beams at wavelengths of 657 nm (RCL-300-656; Crystalaser), 561 nm (Sapphire 561-250; Coherent), 532 nm (GCL-200-L; Crystalaser), 514 nm (Sapphire 514-50; Coherent), 460 nm (Sapphire 460-10; Coherent) and 405 nm (CUBE 405-50C; Coherent) were individually controlled by mechanical shutters (Uniblitz LS6T2; Vincent Associates) and an acousto-optic tunable filter (AOTF PCAOM NI VIS; Crystal Technology). All laser lines were combined and coupled into an optical fiber (Oz Optics), and the fiber output was collimated and focused on the back focal plane of a high numerical aperture (NA) oil immersion objective (100x UPlanSApo, NA1.4; Olympus). Here, since CCPs are primarily located at the plasma membrane, we used a total-internal-reflection-fluorescence (TIRF) or highly-oblique-incidence imaging geometry to reduce background fluorescence, but note that such geometry is not a general requirement for 3D STORM, which allows wide field imaging with a depth of a few microns[24]. The fluorescence emission was collected by the same objective and imaged onto a back-illuminated EMCCD camera (iXON DU-860 or iXON DU-897; Andor). To stabilize the focus during data acquisition, an 830 nm fiber-coupled diode laser (LPS-830-FC; Thorlabs) was introduced into the microscope in a separate objective-type TIRF path. The reflected IR beam from the coverglass-water interface was directed to a quadrant photodiode. The position readout of the quadrant photodiode provided feedback to a piezo objective positioner (Nano-F100; MadCity Labs), keeping the focal drift to less than 20 nm.

For single-color imaging of Alexa647, the probes were activated by the 405 nm laser and the activated Alexa647 molecules were imaged with a 657 nm laser. The excitation beams were reflected by a dichroic longpass mirror (T660LPXR; Chroma) and the fluorescence emission

was filtered with a bandpass filter (ET705/72m; Chroma). For live cell imaging, 657 nm intensity at   15 kW/cm^2 (at the sample) was used to record movies at a frame rate of 500 Hz (iXON DU-860). The intensity of the 405 nm activation laser (2 – 4 orders of magnitude weaker than the 657 nm light) was ramped up to compensate for loss of dyes due to photobleaching when needed.

Atto655 was imaged with a 657 nm laser as in the case of Alexa647 but at a lower intensity (~6 kW/cm^2). For imaging of tdEos, mEos and TMR, the probes were imaged with a 561 nm laser (~5 kW/cm^2). The laser was reflected off by a dichroic longpass mirror (Di01-R561; Semrock) and the fluorescence emission was filtered with a bandpass filter (FF01-617/73; Chroma). Increasing the imaging laser intensity caused a significant reduction in the number of localizations attainable and consequently a lower imaging quality. Like in the case of Alexa647 imaging, the probes were activated by the 405 nm laser, the intensity of which was ramped up to compensate for loss of dyes due to photobleaching when needed. OregonGreen was imaged with a 514 nm beam (~1 kW/cm^2, maximum power available on our setup) reflected by a dichroic longpass (FD520-Di02; Semrock) and the fluorescence was filtered by a bandpass filter (FF01-578/105; Semrock). The fluorescence images were obtained at 100–150 Hz.

For two-color imaging of the Alexa405-Alexa647 and Cy3-Alexa647 probes, we used an alternating activation sequence of 405 nm and 532 nm laser pulses for activating the Alexa405-Alexa647 and Cy3-Alexa647 probes, respectively[23]. The activated Alexa647 molecules were again imaged with a 657 nm laser. For two-color imaging of Alexa647 and Alexa568, two imaging beams (561 nm and 657 nm) and an activation beam (405 nm) were reflected by a custom-designed polychroic mirror (z405/561/657rpc; Chroma). Fluorescence emissions from Alexa647 and Alexa568 were separated by a 630 nm longpass dichroic mounted on a commercial beamsplitting device (Dual-View; Photometrics). The short-wavelength channel was filtered with a bandpass filter (FF01-607/70; Semrock) for Alexa568. The long-wavelength channel was filtered with a bandpass filter (ET705/72m; Chroma) for Alexa647. In addition to the bandpass filters, a double notch filter (NF01-568/647; Semrock) was added before the Dual-View to block the two excitation beams. The two images were each imaged onto 128 × 128 pixels in the EMCCD camera (iXON DU-860) running at 500Hz.

For 3D localization, a cylindrical lens with a focal length of 50 cm (for imaging with the iXON DU-860 camera) or 100 cm (for imaging with the iXON DU-897 camera) was inserted into the imaging optical path[26].

Image analysis

STORM images were generated using similar methods as previously described[26]. Briefly, images of individual molecules were identified and fit to an elliptical Gaussian function to obtain the centroid position coordinates (x_0 and y_0) and the Gaussian widths (d_x and d_y). The lateral position of the molecule were determined as x_0 and y_0, while the z position was calculated from d_x and d_y using a calibration curve independently determined by imaging 100 nm fluorescent bead (Tetraspeck; Invitrogen) on a coverglass while scanning in z. The z

position was then corrected for refractive index mismatch between glass and the imaging medium as previously described[24].

We considered other factors that could potentially make single-molecule images appear elliptical, such as the polarized emission of dyes with fixed dipole orientations, which could contribute to the z localization error. In our experiments, individual molecular images did not appear elliptical in the absence of the cylindrical lens and the measured residual ellipticity resulted in a $z = 17$ nm, which is well within our z-localization precision for all probes, indicating that the z-dependent astigmatism was the primary source of ellipticity.

Sample drift during the image acquisition in both lateral and axial directions was measured and corrected by two means as described previously[26]: (1) correlation function of the image itself for fixed-cell images; (2) traces of fiducial markers for long (>50 sec) time series of live cells. Sample drift was negligible in live-cell images of shorter durations.

In two-color images of immunostained samples in Supplementary Fig. 1(a–c), where the probes were distinguished by the activation wavelength, the color crosstalk due to nonspecific activation or false activation was subtracted as described previously[23]. For two-color imaging of Alexa647 and Alexa568, the two STORM images were aligned by a 3rd order polynomial warping map in 3D obtained from calibration images of 100 nm Tetraspeck fluorescent beads. The residual alignment error is ~7 nm in xy and ~15 nm in z.

Cell autofluorescence and out-of-focus or non-specifically bound fluorescent molecules give background in the STORM images, which appeared as scattered localizations at low local densities. To remove the background noise, STORM images were filtered according to the local density of localizations. This treatment has the same function as background subtraction in conventional fluorescence imaging. Briefly, for each localization, the number of neighboring localizations was counted within a circular (for 2D images) or a spherical (for 3D images) region of a finite diameter of 50 – 80 nm to determine the local density of this localization. Localizations with local densities less than a specified cutoff value (2 – 5) were removed. As an example, Supplementary Fig. 10 shows the comparison of the STORM images of a coated pit containing transferrin with and without density filtering. The image with density filtering is also shown in Supplementary Fig. 1c. Subsequent analyses on size distribution and Nyquist resolution were performed on the density-filtered images.

To determine the localization precision of the six probes, we imaged fluorescent beads with a diameter of 100 nm. Localization accuracy of each probe is calculated from the FWHM of localization distribution of individual beads. We adjusted the imaging laser intensity such that the average photon number detected from the beads per imaging frame was identical to the average photon number of the probe per switching cycle. This method was used because the photoactivable mEos2 and tdEos produce 1–2 localization per molecule, which does not allow the measurement of localization precision from multiple localizations of the same molecules. For photoswitchable probes with multiple cycles, such as Alexa647, multiple localizations obtained from a single molecule can be used to determine the localization instead, which yielded similar results as the bead measurements. In the main text and Supplementary Table 1, we report the average localization precision over the 300 nm

imaging depth. We found that, for all seven probes studied here, the *xy* localization precision changed only slightly with the *z* position and that the measured values in all *z* ranges were within 20% of the average value. The *z* localization precision of the brighter probes, Alexa647 and Alexa568, also varied only slightly (within 13% of the average value for Alexa647 and within 20% for Alexa568). For the probes with relatively low photon numbers, such as EosFP, Atto655, TMR and Oregon Green, the variation of the *z* localization precision was more significant: at $z = 0$, 100, 200, and 300 nm, the localization precisions were 74%, 81%, 107%, 138% of the average value. Because most of the structures of interest (transferrin clusters and CCPs) were within the range of $z = 0 - 200$ nm, the variation in localization precision was even smaller.

To quantitatively compare spatial resolution of different probes, we reported convolved resolutions computed as $[(\text{localization precision})^2 + (\text{Nyquist resolution})^2]^{1/2}$. When localization precision and Nyquist resolution differ substantially, the resolution is limited by the larger of the two. When the localization accuracy and Nyquist resolution are comparable, both factors contribute significantly and the convolved resolution provides a good measure of the overall resolution.

Supplementary Material

Refer to Web version on PubMed Central for supplementary material.

Acknowledgments

References

1. Hell SW. Far-field optical nanoscopy. Science. 2007; 316:1153–1158. [PubMed: 17525330]

2. Huang B, Babcock H, Zhuang X. Breaking the diffraction barrier: super-resolution imaging of cells. Cell. 2010; 143:1047–1058. [PubMed: 21168201]

3. Klar TA, Hell SW. Subdiffraction resolution in far-field fluorescence microscopy. Opt Lett. 1999; 24:954–956. [PubMed: 18073907]

4. Heintzmann R, Jovin TM, Cremer C. Saturated patterned excitation microscopy -a concept for optical resolution improvement. J Opt Soc Am A. 2002; 19:1599–1609.

5. Gustafsson MGL. Nonlinear structured-illumination microscopy: Wide-field fluorescence imaging with theoretically unlimited resolution. Proc Natl Acad Sci U S A. 2005; 102:13081–13086. [PubMed: 16141335]

6. Rust MJ, Bates M, Zhuang X. Sub-diffraction-limit imaging by stochastic optical reconstruction microscopy (STORM). Nat Methods. 2006; 3:793–795. [PubMed: 16896339]

7. Betzig E, Patterson GH, Sougrat R, Lindwasser OW, Olenych S, Bonifacino JS, Davidson MW, Lippincott-Schwartz J, Hess HF. Imaging intracellular fluorescent proteins at nanometer resolution. Science. 2006; 313:1642–1645. [PubMed: 16902090]

8. Hess ST, Girirajan TP, Mason MD. Ultra-high resolution imaging by fluorescence photoactivation localization microscopy. Biophys J. 2006; 91:4258–4272. [PubMed: 16980368]

9. Thompson RE, Larson DR, Webb WW. Precise nanometer localization analysis for individual fluorescent probes. Biophys J. 2002; 82:2775–2783. [PubMed: 11964263]

10. Yildiz A, Forkey JN, McKinney SA, Ha T, Goldman YE, Selvin PR. Myosin V walks hand-over-hand: single fluorophore imaging with 1.5-nm localization. Science. 2003; 300:2061–2065. [PubMed: 12791999]

11. Westphal V, Rizzoli SO, Lauterbach MA, Kamin D, Jahn R, Hell SW. Video-rate far-field optical nanoscopy dissects synaptic vesicle movement. Science. 2008; 320:246–249. [PubMed: 18292304]

12. Hein B, Willig KI, Hell SW. Stimulated emission depletion (STED) nanoscopy of a fluorescent protein-labeled organelle inside a living cell. Proc Natl Acad Sci U S A. 2008; 105:14271–14276. [PubMed: 18796604]

13. Kner P, Chhun BB, Griffis ER, Winoto L, Gustafsson MG. Super-resolution video microscopy of live cells by structured illumination. Nat Methods. 2009; 6:339–342. [PubMed: 19404253]

14. Shroff H, Galbraith CG, Galbraith JA, Betzig E. Live-cell photoactivated localization microscopy of nanoscale adhesion dynamics. Nat Methods. 2008; 5:417–423. [PubMed: 18408726]

15. Hess ST, Gould TJ, Gudheti MV, Maas SA, Mills KD, Zimmerberg J. Dynamic clustered distribution of hemagglutinin resolved at 40 nm in living cell membranes discriminates between raft theories. Proc Natl Acad Sci U S A. 2007; 104:17370–17375. [PubMed: 17959773]

16. Manley S, Gillette JM, Patterson GH, Shroff H, Hess HF, Betzig E, Lippincott-Schwartz J. High-density mapping of single-molecule trajectories with photoactivated localization microscopy. Nat Methods. 2008; 5:155–157. [PubMed: 18193054]

17. Subach FV, Patterson GH, Manley S, Gillette JM, Lippincott-Schwartz J, Verkhusha VV. Photoactivatable mCherry for high-resolution two-color fluorescence microscopy. Nat Methods. 2009; 6:153–159. [PubMed: 19169259]

18. Biteen JS, Thompson MA, Tselentis NK, Bowman GR, Shapiro L, Moerner WE. Super-resolution imaging in live Caulobacter crescentus cells using photoswitchable EYFP. Nat Methods. 2008; 5:947–949. [PubMed: 18794860]

19. Heilemann M, van de Linde S, Mukherjee A, Sauer M. Super-resolution imaging with small organic fluorophores. Angew Chem Int Ed Engl. 2009; 48:6903–6908. [PubMed: 19670280]

20. Wombacher R, Heidbreder M, van de Linde S, Sheetz MP, Heilemann M, Cornish VW, Sauer M. Live-cell super-resolution imaging with trimethoprim conjugates. Nat Methods. 2010; 7:717–719. [PubMed: 20693998]

21. Testa I, Wurm CA, Medda R, Rothermel E, von Middendorf C, Folling J, Jakobs S, Schonle A, Hell SW, Eggeling C. Multicolor fluorescence nanoscopy in fixed and living cells by exciting conventional fluorophores with a single wavelength. Biophys J. 2010; 99:2686–2694. [PubMed: 20959110]

22. Klein T, Loschberger A, Proppert S, Wolter S, van de Linde S, Sauer M. Live-cell dSTORM with SNAP-tag fusion proteins. Nat Methods. 2011; 8:7–9. [PubMed: 21191367]

23. Bates M, Huang B, Dempsey GT, Zhuang X. Multicolor super-resolution imaging with photo-switchable fluorescent probes. Science. 2007; 317:1749–1753. [PubMed: 17702910]

24. Huang B, Jones SA, Brandenburg B, Zhuang X. Whole-cell 3D STORM reveals interactions between cellular structures with nanometer-scale resolution. Nat Methods. 2008; 5:1047–1052. [PubMed: 19029906]

25. Zhuang X. Nano-imaging with Storm. Nat Photonics. 2009; 3:365–367. [PubMed: 20300445]

26. Huang B, Wang W, Bates M, Zhuang X. Three-dimensional super-resolution imaging by stochastic optical reconstruction microscopy. Science. 2008; 319:810–813. [PubMed: 18174397]

27. Juette MF, Gould TJ, Lessard MD, Mlodzianoski MJ, Nagpure BS, Bennett BT, Hess ST, Bewersdorf J. Three-dimensional sub-100 nm resolution fluorescence microscopy of thick samples. Nat Methods. 2008; 5:527–529. [PubMed: 18469823]

28. Pavani SRP, Thompson MA, Biteen JS, Lord SJ, Liu N, Twieg RT, Piestuna R, Moerner WE. Three-dimensional, single-molecule fluorescence imaging beyond the diffraction limit by using a double-helix point spread function. Proc Natl Acad Sci U S A. 2009; 106:2995–2999. [PubMed: 19211795]

29. Shtengel G, Galbraith JA, Galbraith CG, Lippincott-Schwartz J, Gilletted JM, Manley S, Sougrat R, Waterman CM, Kanchanawonge P, Davidson MW, Fetter RD, Hess HF. Interferometric

fluorescent super-resolution microscopy resolves 3D cellular ultrastructure. Proc Natl Acad Sci U S A. 2009; 106:3125–3130. [PubMed: 19202073]

30. Tang J, Akerboom J, Vaziri A, Looger LL, Shank CV. Near-isotropic 3D optical nanoscopy with photon-limited chromophores. Proc Natl Acad Sci U S A. 107:10068–10073. [PubMed: 20472826]

31. Dempsey GT, Bates M, Kowtoniuk WE, Liu DR, Tsien RY, Zhuang X. Photoswitching mechanism of cyanine dyes. J Am Chem Soc. 2009; 131:18192–18193. [PubMed: 19961226]

32. Egner A, Geisler C, Von Middendorff C, Bock H, Wenzel D, Medda R, Andresen M, Stiel AC, Jakobs S, Eggeling C, Schonle A, Hell SW. Fluorescence nanoscopy in whole cells by asynchronous localization of photoswitching emitters. Biophys J l. 2007; 93:3285–3290.

33. Sako Y, Kusumi A. Barriers for lateral diffusion of transferrin receptor in the plasma membrane as characterized by receptor dragging by laser tweezers: fence versus tether. J Cell Biol. 1995; 129:1559–1574. [PubMed: 7790354]

34. Rust MJ, Lakadamyali M, Zhang F, Zhuang X. Assembly of endocytic machinery around individual influenza viruses during viral entry. Nat Struct Mol Biol. 2004; 11:567–573. [PubMed: 15122347]

35. Keppler A, Gendreizig S, Gronemeyer T, Pick H, Vogel H, Johnsson K. A general method for the covalent labeling of fusion proteins with small molecules in vivo. Nat Biotechnol. 2003; 21:86–89. [PubMed: 12469133]

36. Gaidarov I, Santini F, Warren RA, Keen JH. Spatial control of coated-pit dynamics in living cells. Nat Cell Biol. 1999; 1:1–7. [PubMed: 10559856]

37. McNeil PL, Warder E. Glass beads load macromolecules into living cells. J Cell Sci. 1987; 88:669–678. [PubMed: 2459146]

38. McKinney SA, Murphy CS, Hazelwood KL, Davidson MW, Looger LL. A bright and photostable photoconvertible fluorescent protein. Nat Methods. 2009; 6:131–133. [PubMed: 19169260]

39. Wiedenmann J, Ivanchenko S, Oswald F, Schmitt F, Rocker C, Salih A, Spindler KD, Nienhaus GU. EosFP, a fluorescent marker protein with UV-inducible green-to-red fluorescence conversion. Proc Natl Acad Sci U S A. 2004; 101:15905–15910. [PubMed: 15505211]

40. Fernandez-Suarez M, Ting AY. Fluorescent probes for super-resolution imaging in living cells. Nat Rev Mol Cell Biol. 2008; 9:929–943. [PubMed: 19002208]

41. Lakadamyali M, Rust MJ, Zhuang X. Ligands for clathrin-mediated endocytosis are differentially sorted into distinct populations of early endosomes. Cell. 2006; 124:997–1009. [PubMed: 16530046]

42. Nugent-Glandorf L, Perkins TT. Measuring 0.1-nm motion in 1 ms in an optical microscope with differential back-focal-plane detection. Opt Lett. 2004; 29:2611–2613. [PubMed: 15552661]
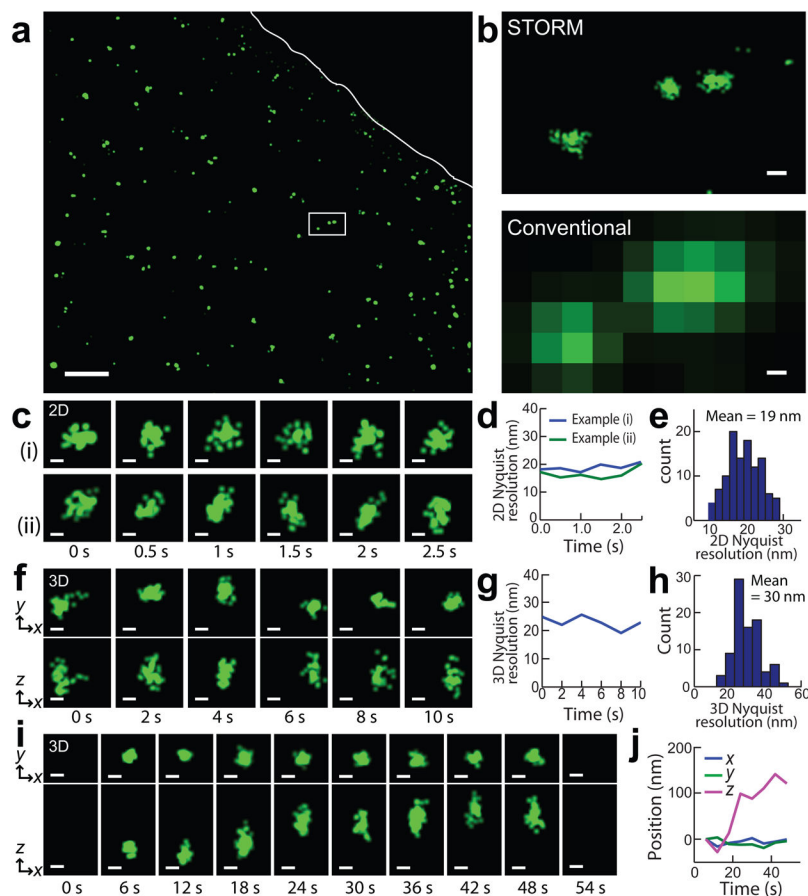
Figure 1. STORM images of transferrin in live cells
(**a**) A wide-field 2D STORM image. Analysis was limited to inside the cell boundary, demarcated by the white line, due to unreliable STORM localizations outside the cell caused by fluorescence background from diffusing transferring molecules. (**b**) The zoomed-in comparison between 2D STORM (upper panel) and conventional (lower panel) images of the boxed region in (**a**). (**c**) Examples of two transferrin clusters, each showing six consecutive 2D STORM snapshots (0.5 sec per snapshot). (**d**) The 2D Nyquist resolution for the examples shown in (**c**). (**e**) A histogram of Nyquist resolutions constructed from many individual transferrin clusters at 0.5-sec time resolution. (**f**) Consecutive 3D STORM snapshots of a transferrin cluster (2 sec per snapshot). Upper row: *xy* projections. Lower row: *xz* projections. (**g**) The 3D Nyquist resolution derived from the snapshots in (**f**). (**h**) A histogram of 3D Nyquist resolutions, constructed from many clusters at 2-sec time resolution. (**i**) Images of a transferrin cluster at 6 sec/snapshot at 34°C showing its time evolution, starting from formation (6 sec) to disappearance (54 sec) upon internalization. Upper row: *xy* projections. Lower row: *xz* projections. (**j**) The *x*, *y* and *z* coordinates of the centroid position of the transferrin cluster in (**i**). Scale bars, 2 μm (**a**), 100 nm (**b**), 50 nm (**c**,**f**,**i**). In all figures, the *z* axis points away from the glass substrate.
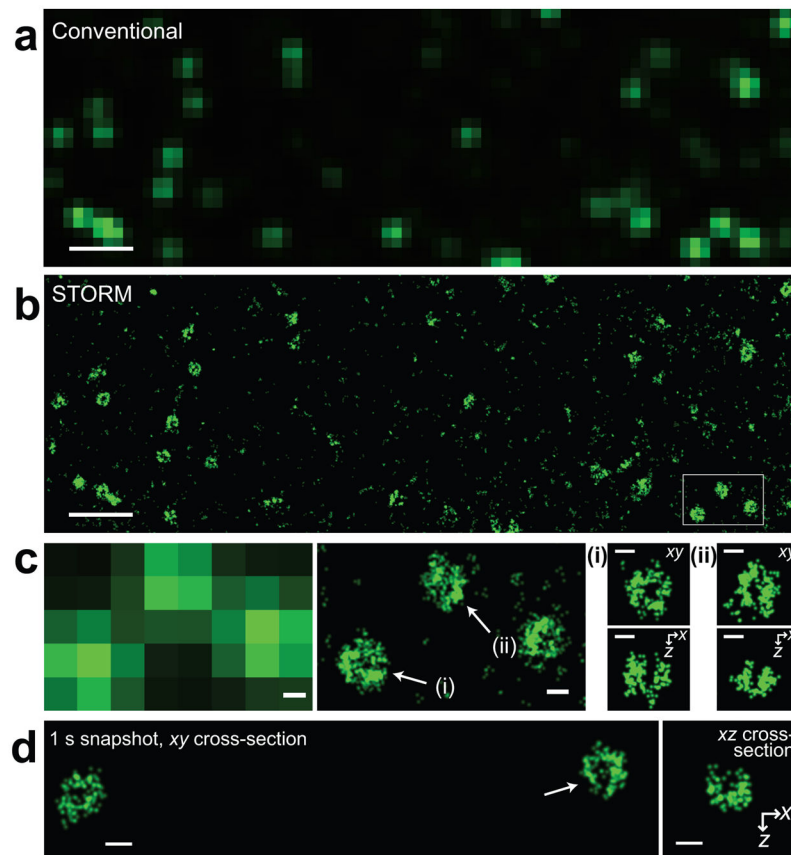
Figure 2. 3D STORM images of clathrin-coated pits (CCPs) labeled with photoswitchable cyanine dyes via a SNAP tag in live cells

(**a**) Conventional wide-field image of CCPs in a live cell. (**b**) 3D STORM image of the same area taken in 30 seconds. Here, only the *xy* projection is shown. (**c**) Zoomed-in conventional (left panel) and 3D STORM (center panel) images of the boxed region in (**b**). The 3D STORM image is again presented as the *xy* projection. Right panels: Cross-sections of the CCPs indicated in the center panel. Upper row: an *xy* cross-section near the plasma membrane. Lower row: an *xz* cross-section cutting through the middle of the pit. (**d**) 3D STORM image of CCPs taken in 1 second. Left panel: *xy* cross-section of two CCPs. Right panel: *xz* cross-section of the CCP indicated by the arrow. Scale bars, 1 μm (**a**,**b**), 100 nm (**c**,**d**).
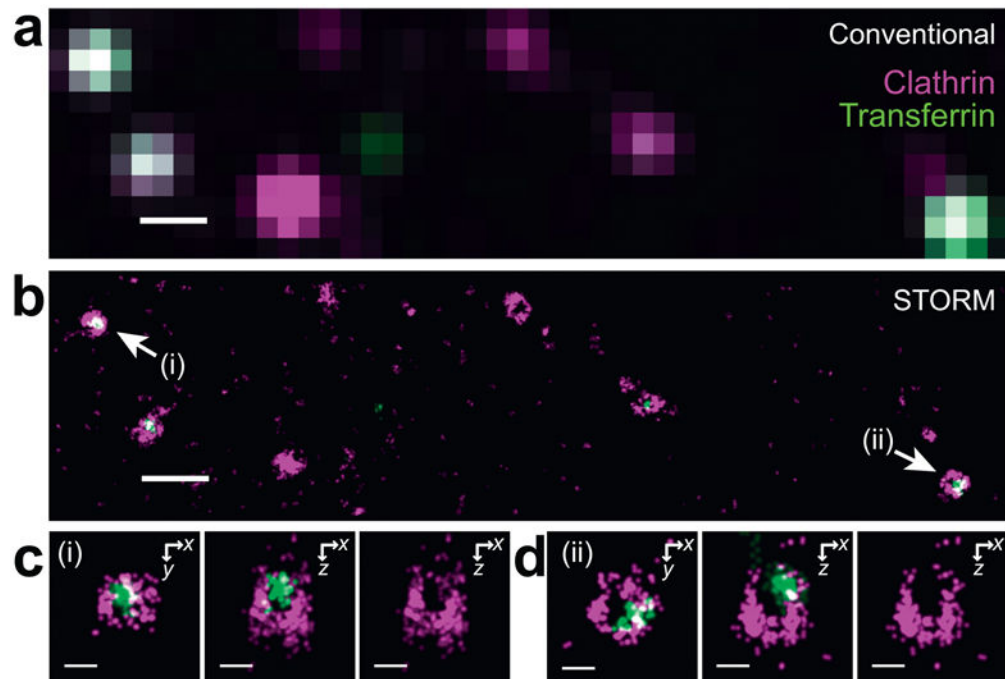
Figure 3. Two-color 3D STORM images of CCPs and transferrin in live cells
CCPs are labeled with Alexa647 via a SNAP tag (magenta) and transferrin is directly labeled with Alexa568 (green). (**a**) Conventional image of CCPs and transferrin in a live cell. (**b**) 3D STORM image of the same area taken in 30 seconds. The *xy* projection of the 3D image is displayed. (**c,d**) Zoomed-in STORM images of the CCPs indicated in (**b**). Left panel: the *xy* cross-section near the plasma membrane. Center panel: *xz* cross-section cutting through the middle of the invaginating pit. Right panel: corresponding *xz* cross-section of the clathrin channel only. Scale bars, 500 nm (**a,b**), 100 nm (**c,d**).
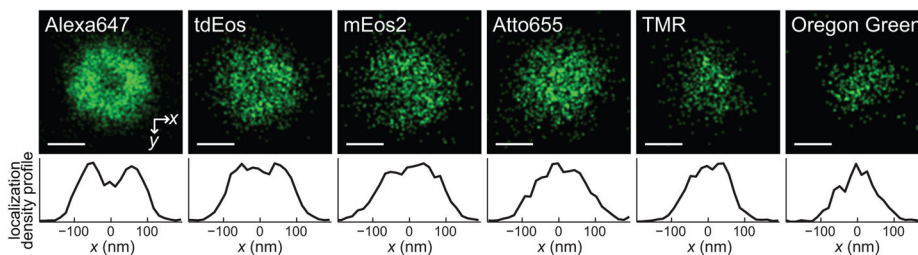
Figure 4. Comparison of CCPs labeled with various probes
Composite CCPs constructed by aligning the 3D center-of-mass of CCPs in an entire field of view for each probe. A portion of the field of view is displayed in Fig. 2b for Alexa647 and in Supplementary Fig. 8 for tdEos, mEos2, Atto655, TMR and Oregon Green. The *xy* cross-sections through the 3D center of the composite CCPs are displayed in the upper panels. The localization density profiles along the *x* axis within a 75-nm wide stripe at the center of the pits are shown in the lower panels. Scale bar, 100 nm.